International Journal of
MATERIALS RESEARCH

Zeitschrift für METALLKUNDE

Original Contributions

Rike Yudianti[a], Lektro Ganda Hutabarat[b], Yuyun Irmawati[a], Henry Widodo[a], Nanik Indayaningsih[a], Awan Magfirah[b]

[a] Research Centre for Physics, Indonesian Institute of Sciences, Kawasan Puspiptek, South Tangerang, Indonesia
[b] Physics Department, North Sumatera University, Medan, North Sumatera, Indonesia

Carbon nanotube network as an electron pathway in nanocomposite films

The role of a multiwalled carbon nanotube (MWCNT) network embedded in polymer nanocomposite is a key factor to study. Polyvinyl alcohol was used as the polymer matrix for 0.1–0.4 wt.% functionalised nanotubes in an effort to establish the nanotube's role in nanocomposite films. The fabrication of nanocomposite film was conducted using an easy and simple procedure via the casting technique. Nanocomposite properties show that in the early addition of 0.1 wt.% MWCNT, an isolator–semiconductor transition with 1.1×10^{-8} S cm^{-1} conductivity occurred. Nanocomposite films were shown to be sensitive to UV light at 250–400 nm and tended to have a high transmission (approximately ~90 %) within the visible region. Additionally, an MWCNT concentration of 0.3 wt.% in the electron pathway carried charge carriers of approximately 2.1×10^{-7} S cm^{-1} via a complete electrically-conductive path. As such, the network nanotubes displayed extraordinary properties as reinforcement for nanocomposite films when viewed in terms of mechanical strength and elongation increased in respective ranges of 7.3–18.8 % and 14.9–25.02 %. Upshift of the G-band occurred at approximately 7–26 cm^{-1}, which was indicative of an electron transfer between the nanotube and the matrix.

Keywords: Carbon nanotube; Nanocomposite; Electron pathway

1. Introduction

In addition to being lightweight, polymers possess a variety of useful physical properties, such as mechanical flexibility, optical transparency and an increased resistance to corrosion. This enables them to be used for diverse applications, including as medical materials, electronic devices, packaging and as functional composites [1]. Recently, flexible electronic films have become high-demand materials for the production of sensors, displays, solar cells and electronic devices because carbon nanotubes (CNTs) generally exhibit good electrical, mechanical, optical, and thermal conductive properties, which, in turn, make them effective electrocatalysts [2, 3], photocatalysts [4–6], highly sensitive nanocomposites [7, 8], thermoelectric nanocomposite [9–11], humidity, gas and liquid sensing [12, 13] and strain-sensing film [14, 15]. Although achieving maximum dispersion of the CNT in a polymer matrix poses a significant challenge to researchers, there are extraordinary advantages to be enjoyed in accomplishing this feat, particularly as it relates to the development of new materials. On a macroscopic level, high performance polymer-CNT composites have properties similar to the individual CNTs from which they are made. Additionally, some polymers offer selective advantages only when incorporated into a CNT, which makes them attractive materials for reinforcement. Mahore et al. demonstrated the role of CNTs in increasing the specific capacitance of polypyrrole (PPy)/CNT nanocomposites in comparison with their pure PPy counterparts [16]. Arash B et al. reported carbon nanotube reinforced poly(methyl methacrylate) (PMMA) matrix composites by evaluating their fractural behaviour [17]. Additionally, extensive research has been conducted on incorporating CNTs into many polymer matrices, i.e. P(MMA-co-EMA), epoxy and elastomer poly(dimethylsiloxane) nanocomposites [18–20].

Over the last few decades, the generation of flexible, transparent films from nano-cellulose has attracted interest due to the raw materials' abundance and extraordinary renewability. Unfortunately, synthesis requires time-consuming and complex chemical processes, which are neither effective nor cost-efficient [21–23].

In recent studies, polyvinyl alcohol (PVA) was found to be highly processable. To this end, transparent polymer matrices made from this material have been receiving renewed interest for the manufacture of polymer nanocomposites. Flexible, transparent and conductive PVA-MWCNT nanocomposite films are easily prepared via simple procedures with little to no chemical waste afterwards. Researchers have also found that formation of the MWCNT network within a PVA matrix builds extensive interfacial bonds between the various PVA-MWCNTs, which in turn promotes electron interactions and ultimately improves the performance of the nanocomposite film they are used to manufacture. A series of performance analyses, i.e. electrical conductivity, optical transparency, structural nanocomposite and mechanical properties, is presented in this study in an effort to understand the nanotube network of these types of materials in more detail. We found that low concentrations of randomly distributed nanotubes within the film caused measurable changes in the electrical properties of the matrix which were proportionally related to the film's optical and mechanical properties.

2. Experimental procedure

2.1. Synthesis of nanocomposite film

MWCNT was purchased from Chengdu Alpha Nano Tech. Co. Ltd. with a purity level of 95%, an outer diameter of 50 nm and a length of 5 μm. MWCNT, which was used as a filler in reinforced polymer nanocomposites, was acid-functionalised according to the experimental procedure reported by Yudianti et al. [24]. Polyvinyl alcohol (PVA), which was purchased from Sigma Aldrich, was used as the polymer matrix. Well-dispersed functionalised CNT (10 mg) in 100 mL DI water was first prepared via ultrasonication over the course of 4 h. The PVA solutions (10 w/v) were then prepared by dissolving in DI water at 90 °C. Under mechanical stirring at 400 rpm and at 23 °C, the dispersed CNT solution was slowly dripped into various PVA solutions at concentrations of 0.1, 0.2, 0.3 and 0.4% (w/w). After mixing, the solutions were sonicated for 2 h to achieve uniform and stable dispersion of MWCNT. The homogenised solution was cast onto a Teflon plate and dried in an oven at 60 °C for 5 h. For scientific comparison, pure PVA films were also prepared (Fig. 1).

2.2. Characterisation and testing of nanocomposite film

2.2.1. Hydrophobic properties of nanocomposite film

Contact angle measurements were manually performed using a modified contact angle analyser. Measurements were repeated in triplicate at different surface points and were carried out with water droplets (2 μL) using a micropipette. The contact angle measurements were recorded as snapshots for a single water drop and were measured for each surface point. Average and standard deviation values were calculated.

2.2.2. Transparency testing of nanocomposite film

UV–Vis absorbance of the nanocomposite films (2×2 cm^2) were measured using a UV–Vis Ocean Optic 2000proin spectrometer within the range of 250–1 100 nm.

2.2.3. Topographical surface by AFM imaging.

To study homogeneity and surface roughness, the nanocomposite films (1 cm^2) were analysed using an atomic force microscope (AFM) (Bruker Nano 9).

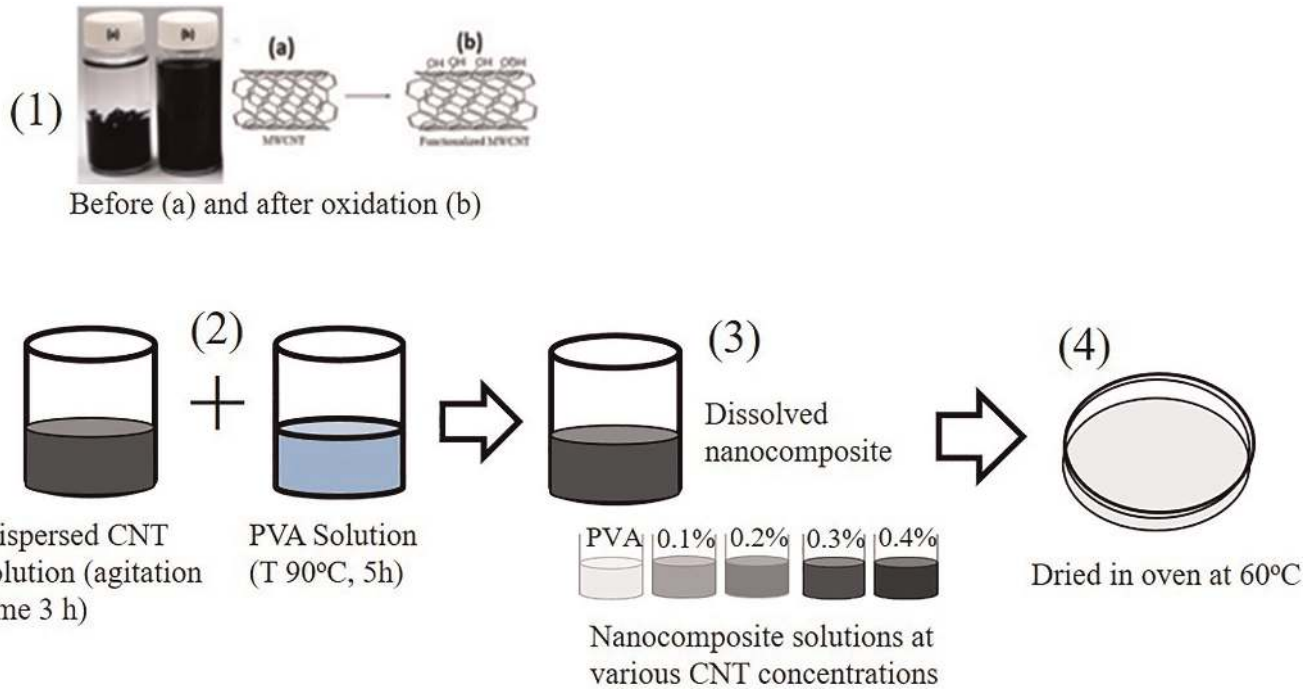

Fig. 1. Fabrication of nanocomposite film.

2.2.4. Mechanical properties of nanocomposite film

Dumbbell-shaped nanocomposite films were cut in dimensions according to ASTM D412. Using a Universal Testing Machine (Tensometer LLOYD 2000R), the mechanical properties of the nanocomposite films, i.e. tensile strength and elongation, were measured until break-point was reached in an effort to establish the maximum tensile strength of the material. Five nanocomposite specimens (2.0×4.0 cm^2) were repeatedly stretched at a constant load speed of 0.2 mm min^{-1} until the specimens cracked. Mechanical strain readings were recorded using a computer connected to the control unit of the tensile apparatus. The tensile strength of the samples was estimated and plotted on a stress–strain graph.

2.2.5. DC conductivity of nanocomposite film

The DC conductivity of the film was measured using a Fluke-1587 FC Insulation meter. The measurement was conducted at room temperature with the average thickness of the film being approximately 95 µm.

2.2.6. Raman spectroscopy analysis of nanocomposite

Raman spectroscopy was carried out using Horiba XploRA Plus Nd:YAG laser with 532 nm wavelength for excitation, a light spot diameter of 0.1 mm and at a resolution of 4 cm^{-1}. The Raman spectra were recorded using a microscope equipped with a triple monochromator and a Peltier-cooled charge couple detector. Raman measurements were conducted in powder form for MWCNT and in film form for both the PVA and the nanocomposite materials.

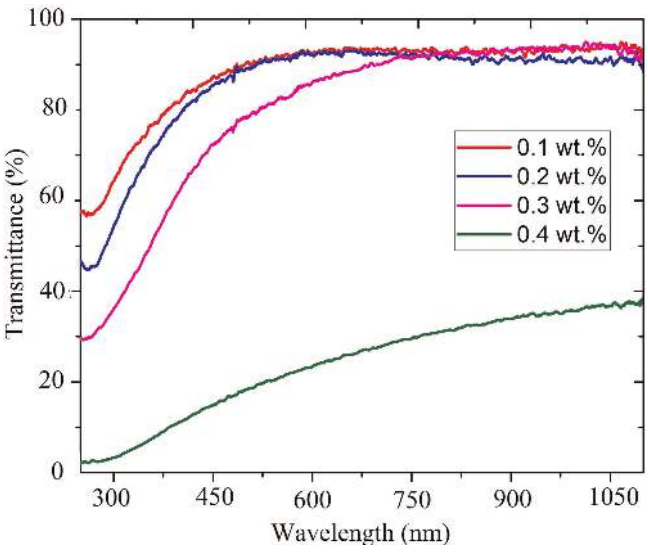

Fig. 2. Effect of CNT concentration on film transparancy.

3. Results and discussion

Understanding interfacial CNT/PVA interactions at various CNT concentrations is essential for accurately predicting the external and internal factors that effect changes in the optical transparency, structural, electrical and mechanical properties of nanocomposites (Figs. 2 and 3). Figure 2 shows the transparency of our nanocomposite films at various weight ratios. As observed, the nanocomposites had different optical responses over a range of 250 – 1 000 nm; the films were shown to generally possess high transparency within the visible and near IR regions, but low transparency near the UV region. The MWCNTs under investigation also exhibited peak absorption at 250 nm, which corresponded to the intrinsic optical properties of graphite [25]. Additionally, transparency was shown to be inversely proportional to the concentration of CNT, i.e. increasing the CNT concentration caused the film to darken. Absorbance was found to be directly proportional to the number of particles available for absorbing the energy of the incident light and calculations revealed that this value corresponded to the principles of the Lambert–Beer law [26]. Increasing the concentration to 0.4 wt.% sharply reduced transparency of the nanocomposite films in all regions (a resulting plateau was seen), which was proof that CNT bundled systems were not active in the UV region. At higher concentrations, CNT tended to agglomerate as a bundle system which, in turn, led to a reduction in the active surface area. Thus, only individual carbon nanotubes were able to actively absorb incident light in the UV–Vis region [27].

As stated previously, extensive surface interactions between the CNTs and the polymer matrix result in extraordinary properties within the nanocomposite material itself. The initial addition of CNT to the matrix resulted in a slight increase in the tensile strength of the nanocomposite by up to 7.3 % when compared to their pure PVA counterparts. Homogeneous CNT distribution in the polymer matrix adequately reinforced the nanocomposite film. The tensile strength and elongation of the nanocomposite films were shown to increase within the range of 7.3 – 18.8 % and 14.9 – 25.02 %, respectively (when compared to their pure PVA film counterparts) after the addition of 0.1 – 0.4 wt.% CNT. Thus, Fig. 4 shows the role that CNTs play in effectively reinforcing the nanocomposites. The rising tensile strength at low CNT concentrations is a consequence of both good dispersibility and the stress-transfer effects ema-

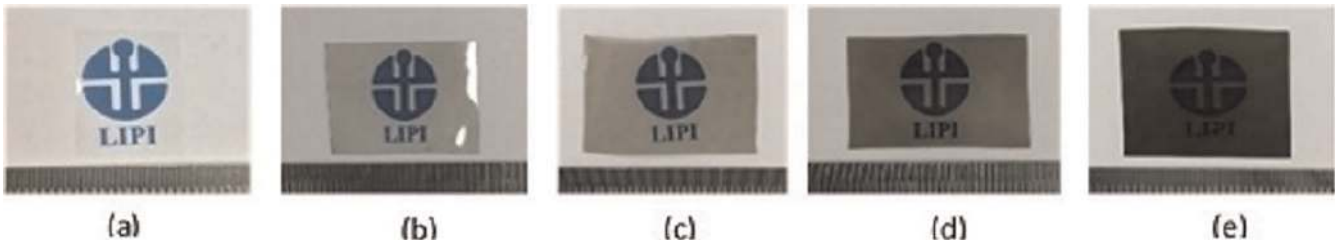

Fig. 3. Appearance of nanocomposite film.

nating from the matrix to the nanotubes. Extensive interfacial interactions between the CNTs and the matrix helped to improve the mechanical properties of the nanocomposites, which then exhibited the rigid fracture features typically seen when elongation of the film decreased at a concentration of 0.4 wt.%. Additionally, Shokrieh et al. found that the tensile strength of the MWCNT/polyester material showed improvements of 6% with the addition of only 0.05 wt.% MWCNT [28]. However, increasing the concentration of nanotubes in the matrix beyond a certain point made the compound brittle, i.e. the number of interfacial interactions between the nanotubes and the matrices declined. This might be because nanotubes tended to agglomerate at higher concentrations (between 0.3 and 0.4 wt.%), which caused inhomogeneity-related stress in our samples. This situation was also seen in the CNT–wood–plastic nanocomposites designed by Zhang et al. (Fig. 5) [29].

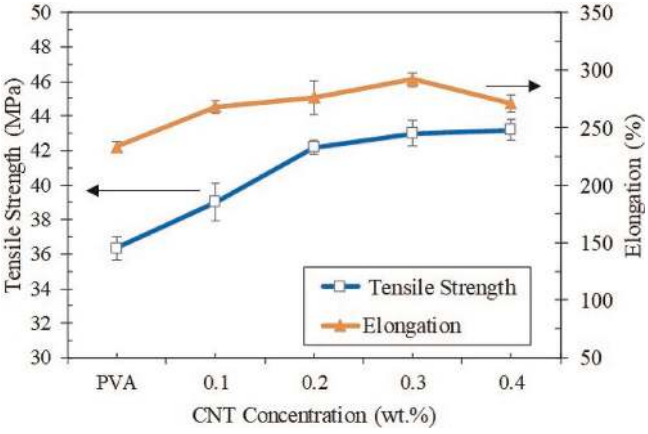

Fig. 4. Effect of CNT concentration on the mechanical properties of nanocomposite film.

SEM imaging was used to understand the morphological surface properties of our nanocomposite materials. We found that whenever the electron beam struck the surface of sample during readings, destruction of the polymer surface occurred and the subsequent changes in the morphological sample prevented us from acquiring clear images. To this end, AFM became the preferred means of acquiring topographic images of our samples. Generally, the surface looked homogeneous and smooth at concentrations ranging from 0.1–0.2 wt.%. The concentration distribution of the MWCNTs was covered by the polymer matrix and they were isolated from each other within the polymer network. At concentrations ranging from 0.3–0.4 wt.%, homogeneity broke down and rough surfaces were seen across the samples. White patches were observed, especially in areas where the polymer matrix concentration was the highest, and were thought to arise from the continuous emergence of the nanotube network at points where the nanotube network formed a junction within the polymer matrix. By increasing the concentration in the matrix, the nanotube network tended to form bundles which depressed the properties of the nanocomposite's system. The occurrence of white flocking on the surface was allegedly the result of matrix flocking, which then acted as a barrier nanotube charge junction.

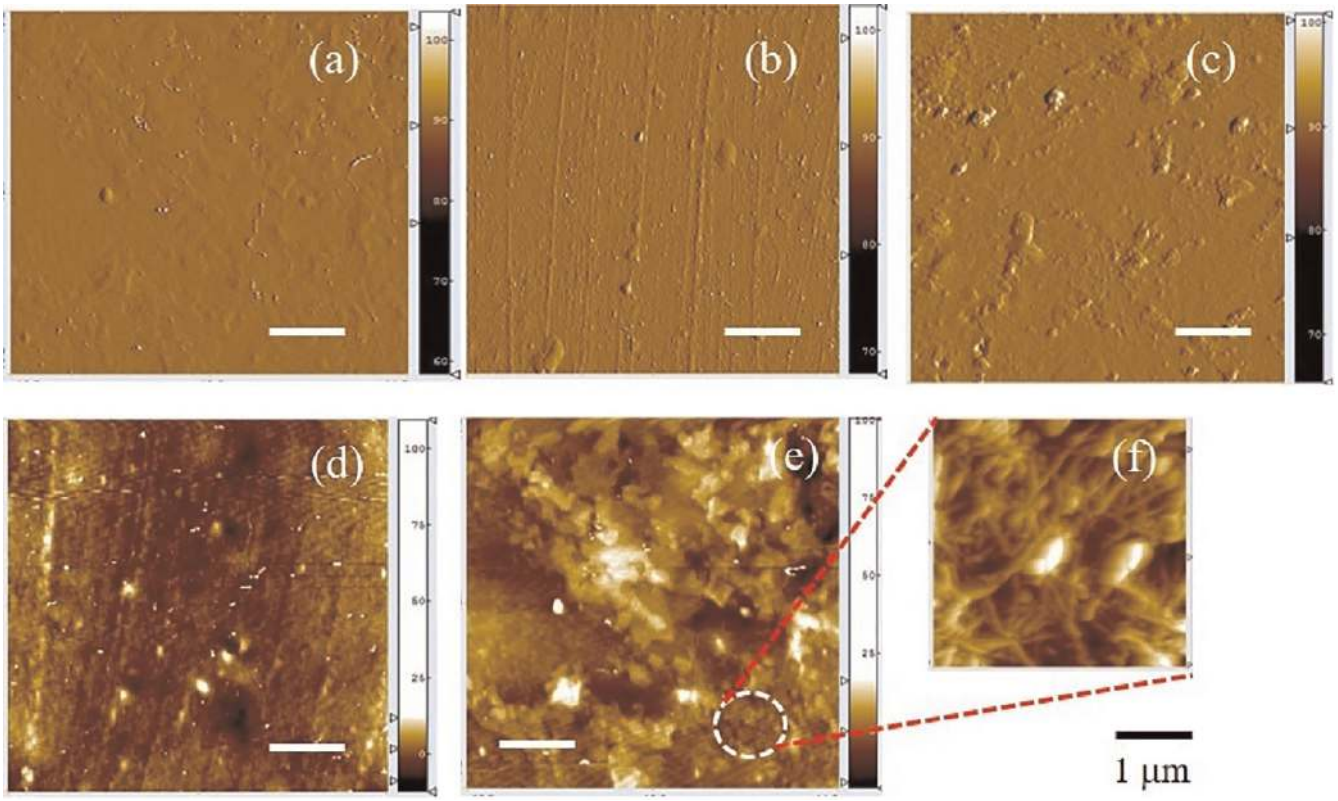

Fig. 5. AFM images of PVA and nanocomposite film at various concentrations of MWCNT (a) PVA Film, (b) 0.1 wt.%, (c) 0.2 wt.%, (d) 0.3 wt.%, (e) 0.4 wt.%, (f) Bundled nanotube.

Schematics of the nanotube network with random orientations in the nanocomposite film under investigation are illustrated in Fig. 6. The pure film had immeasurable conductivity (<2.2 10^{-9} S cm^{-1}) when compared to the insulator. At low critical concentrations, the nanotubes that were isolated from each other by the matrix and PVA ultimately became a barrier to electron flow. At a critical concentration of 0.1 wt.%, electrons began to migrate throughout the nanotube network and several nanotubes had a contact path within the polymer matrix. Good dispersion of the nanotubes throughout the nanocomposite film at low concentration allowed for satisfactory electron conduction because electrons could now move through barriers that they typically should not have been able to pass through. Under these circumstances, CNT offer the additional advantage of electron tunnelling (red circle, A in Fig. 6) and the nanocomposites can now act as a beginner semiconductor (1.1×10^{-8} S cm^{-1}), especially with the initial addition of CNT (0.1 wt.%). However, adding more MWCNT (0.2 wt.%) caused more electrons to hit the barrier (B), as dictated by the concept of carrier dynamics via tunnel coupling between the carbon nanotubes and the polymer network. By increasing the MWCNT concentration to 0.3 wt.%, nanotubes sufficiently close to each other formed a percolating conductive pathway and the electrical percolation threshold was quickly observed. Thus, electrical conductivity of the nanocomposite material increased significantly. Under these circumstances, transfer electrons began appearing and hitting the barrier, whereas the tunnelling effect was shown to gradually disappear when increasing amounts of CNTs (0.3 wt.%) were added. The electrical percolation threshold was reached at a concentration of 0.3 wt.% CNT at the point when the electrical conductivity reached 10×10^{-8} S cm^{-1} via the electrically-conductive path shown in (C). However, the nanocomposites seen upon the formation of the percolated CNT network had different percolation thresholds within each polymer matrix (Fig. 6) [30, 31]. Thus, at higher filler concentrations, a slight increase in conductivity occurred due to the generation of more electron pathways within the matrix. Higher concentrations led to the formation of the fewest number of connections (at approximately 10.6×10^{-8} S cm^{-1}) in the saturation region at 0.4 wt.% (as shown in D) because CNTs agglomerated much more easily under these conditions. Consequently, after passing the percolation threshold, higher concentrations led to smaller incremental changes in conductivity, which implies that extremely sensitive nanocomposites can be generated when the MWCNT concentration is set close to the percolation threshold. Change of electrical properties of nanocomposite which were determined by low concentration nanotube network in transferring electrons reveal CNT as a promising sensing element for the development of sensors. The excellent sensitivity of CNT to the absorption of molecules on the surface provide the possibility for designing sensors [32]. The principle of these sensors is based on changes in the *V–I* curves of nanotubes as a result of adsorption of specific molecules on their surface. The potential use of CNT in sensor devices is one of their further promising applications in electronics, as mechanical and strain sensing [15], humidity sensing [33], and Raman strain sensing [34].

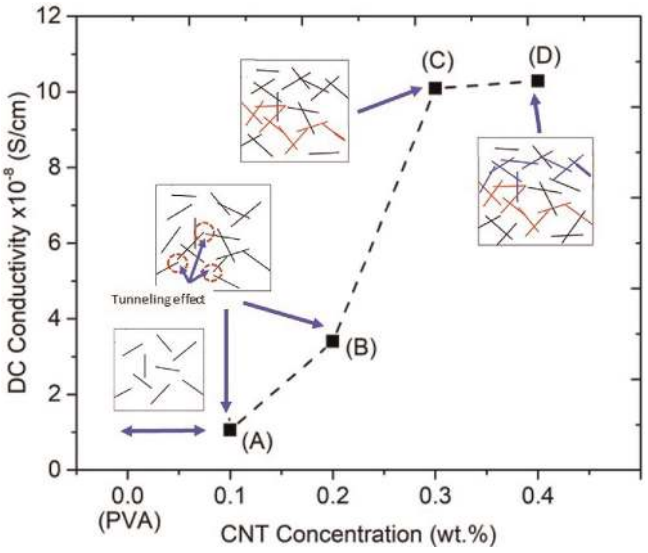

Fig. 6. DC electrical properties of nanocomposites of interest and schematic for CNT pathways within the nanocomposite film.

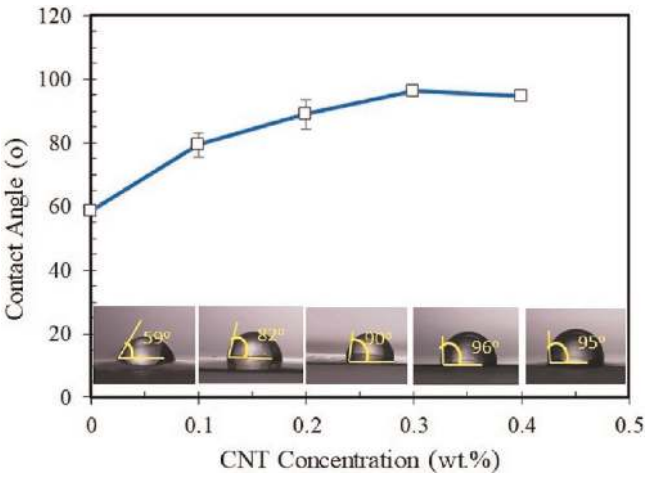

Fig. 7. Hydrophobicity of nanocomposite film.

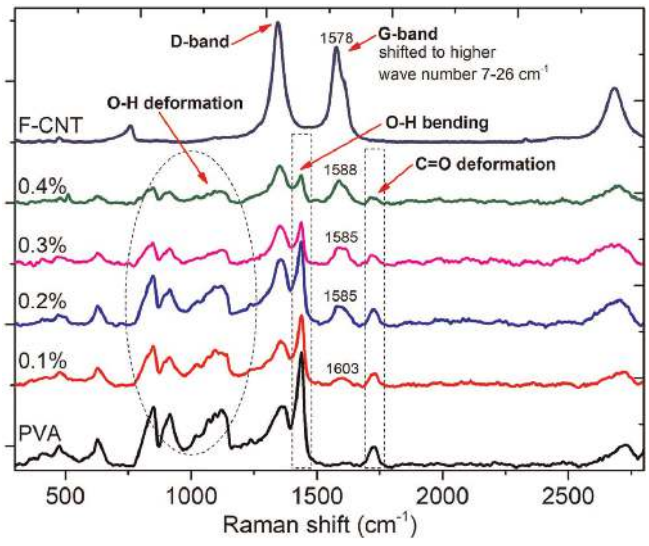

Fig. 8. Raman spectroscopy for nanocomposite film.

The "wettability" of the nanocomposite surface is conventionally monitored using the contact angle measurement system in which readings are performed at room temperature with water as the contact liquid. At the beginning of our study, the contact angle was increased upon the addition of 0.1 wt.% MWCNT and the hydrophobic surface gradually increased from 58° to 79.3° on average. With further addition of MWCNT (up to 0.3 wt.%), hydrophobicity gradually rose to 96.3°, whereas a loss of hydrophobicity was noted at approximately 2 %. Bundled nanotubes at concentrations of 4 wt.% formed stacking free active groups, i. e. hydroxyl and carboxyl nanotubes, which caused a decline in the number of surface interactions between the nanotubes and the polymer matrix. At this concentration, water molecules were absorbed much faster on the surface (Fig. 7), a feature indicative of the importance of adequate CNT dispersion on a macroscopic level. Many previously published studies have also expressed this point when determining the performance of the nanocomposites under investigation [35, 36].

Figure 8 shows that Raman spectroscopy of the nanocomposites when compared with PVA and MWCNT. Two characteristic peaks, typically seen at 1 325 and 1 566 cm^{-1} as the respective ID and IG bands, appeared in the spectra for functionalised MWCNT. ID at 1 325 cm^{-1} corresponded to disordered graphite, an amorphous carbon or defective structure typically found on the sidewalls of MWNTs; on the other hand, IG at 1 566 cm^{-1}, derived from sp^2-bond crystalline carbon, was an indication of ordered structure. The D/G intensity ratio is often considered to be an indicator of the quality of a carbon nanotube sample. According to our calculations, the D/G ratio was shown to increase from 1.25 after acid treatment, a change which could be attributed to the degree of disorder caused by the presence of carboxylate and hydroxyl groups. Evaluation of the relevant intensities of the D and G bands indicated the presence of defects in the carbon nanotubes that were induced via chemical functionalisation. Nanocomposites had peak clusters arising from the PVA as a polymer matrix. The interactions between the nanotubes and environment, i. e. polymer matrix, have a significant effect on the G-band, causing the charge transfer from the MWCNT and matrix of nanotubes [37]. Focusing on the G bands, the nanocomposites were shown to shift toward a higher wave number (approximately 7 – 26 cm^{-1}), which could be attributed to charge transfers between the nanotube and the polymer matrix and could help in describing the extent of the interaction taking place between them. The spectrum of the f-MWCNT standalone exhibits further upshifting when the tubes are embedded in the host matrix as a consequence of disentanglement.

Thus, this result was definitive evidence of MWCNTs' affinity for the PVA matrix. Raman spectroscopy of CNT-based composite materials was used to evaluate the state of dispersion and the extent of the polymer–CNT interactions; these, in turn, were reflected in the shifts or width changes of the peaks. The Raman spectrum of the composite is dominated by the bands of the nanotubes, but some bands of the PVA matrix, in particular, OH deformation; OH bending and C=O bending, are still present. However, no new bands were observed in the PVA/MWCNTs nanocomposite spectra, even though covalent bonding was observed between PVA and the MWCNTs. This situation may have led to improvements in the new characteristics of the nanocomposite's properties.

4. Conclusions

Properties of PVA/MWCNT nanocomposite were successfully investigated. Good dispersion of MWCNT was noted and resulted in changes to the nanocomposite's physical properties on a macroscopic level. When the concentration of nanotubes (0.3 wt.%) in the matrix reached the percolation threshold, the insulating material became conductive. Additionally, the electrically conductive pathways of the MWCNT in the polymer matrix signficantly impacted other physical properties of the nanocomposite material, i. e. hydropobicity, optical and mechanical properties. However, at a concentration of 0.4 wt.%, the nanocomposite of interest became less effective due to diminishing interfacial surface nanotube–polymer interactions in the matrix.

Author Contributions

RY is the main contributor to this manuscript. RY conceived and directed the research design. LH, YI and HW conducted sample preparation and characterisation via optical transparency, mechanical testing, contact angle, and DC conductivity. RY and NI supervised Raman spectroscopy readings, performed data analysis and interpretation. YI plotted UV–Vis spectra, mechanical spectra and Raman spectroscopy. RY and AM supervised experimental work.

The authors are thankful to the Research Centre for Physics for financial support.

References

[1] H.F.B.C. Brinson: "Characteristics, Applications and Properties of Polymers," in Polymer Engineering Science and Viscoelasticity, Switzerland: Springer, Boston, MA, 2018, 55 – 97. DOI:10.1007/978-0-387-73861-1
[2] R. Yudianti, H. Onggo: Nanosci. Nanotechnol. 2 (2012) 171. DOI:10.5923/j.nn.20120206.04
[3] H. Tang, J.H. Chen, Z.P. Huang, D.Z. Wang, Z.F. Ren, L.H. Nie, Y.F. Kuang, S.Z. Yao: Carbon. 42 (2004) 191. DOI:10.1016/j.carbon.2003.10.023
[4] M. Abdel Salam, R.M. Mohamed, A.Y. Obaid: Fullerenes Nanotub. Carbon Nanostructures 22 (2014) 765. DOI:10.1080/1536383X.2012.731584
[5] A.A. Ashkarran, M. Fakhari, H. Hamidinezhad, H. Haddadi, M.R. Nourani: J. Mater. Res. Technol. 4 (2015) 126. DOI:10.1016/j.jmrt.2014.10.005
[6] M.T. Nguyen, C.K. Nguyen, T.M.P. Vu, Q. Van Duong, T.L. Pham, T.C. Nguyen: Adv. Nat. Sci. Nanosci. Nanotechnol. 5 (2014) 0. DOI:10.1088/2043-6262/5/4/045018
[7] S. Luo, Y. Wang, G. Wang, K. Wang, Z. Wang, C. Zhang, B. Wang, Y. Luo, L. Lie, T. Liu: Sci. Rep. 7 (2017) 1. PMid:29180692; DOI:10.1038/srep44056
[8] Z. He, G. Zhou, J. Byun, S. Lee, M. Lim, B. Park, T. Kim, S. Lee, T. Chou: Nanoscale 1000 (2019) 5884. PMid:30869716; DOI:10.1039/c9nr01005j
[9] M. Liebscher, T. Gartner, L. Tzounis, M. Micusik, P Pötschke, M. Stamm, G. Heinrich, B. Voit: Compos. Sci. Technol. 101 (2014) 133. DOI:10.1016/j.compscitech.2014.07.009
[10] L. Tzounis, T. Gartner, M. Liebscher, P. Potschke, M. Stamm, B. Voit, G. Heinrich: Polymer (Guildf). 55 (2014) 5381. DOI:10.1016/j.polymer.2014.08.048
[11] M.S. Zaros Tzounis, M. Laaruti Hegde, Marco Liebscher, Theo Dingemans, Petra Pötschkea, Alkiviadis S.Paipetis, Nikolaos E.Zafeiro poulos: Compos. Sci. Technol. 156 (2018) 158. DOI:10.1016/j.compscitech.2017.12.030

[12] Teng Fei Kai Jiang Fan Jiang Ren Mu Tong Zhang: Appl. Polym. Sci. 131 (2014) 39726. DOI: doi.org/10.1002/app.39726.
[13] D. Maity, K. Rajavel, R. Thangavelu, R. Kumar: Sensors Actuators B. Chem. 261 (2018) 297. DOI:10.1016/j.snb.2018.01.152
[14] S. Wang: thesis, Characterization and analysis of electrical conductivity properties of nanotube composites, Florida State University (2005).
[15] Z. He, J-H. Byun, G. Zhou, B-J. Park, T-H. Kim, S-B. Lee, J-W. Yi, M-K. Um, T-W. Chou: Carbon N. Y. 146 (2019) 701. DOI:10.1016/j.carbon.2019.02.060
[16] R.P. Mahore, D.K. Burghate, S.B. Kondawar: Adv. Mater. Lett. 5 (2014) 400. DOI:10.5185/amlett.2014.amwc.1038
[17] B. Arash, Q. Wang, V.K. Varadan: "nanotube/polymer composites," (2014) 1. DOI:10.1038/srep06479
[18] J. Yang, J. Hu, C. Wang, Y. Qin, Z. Guo: Macromol. Mater. Eng. 289 (2004) 828. DOI:10.1002/mame.200400049
[19] I.S. Hammad Younes, Md. Mahfuzur Rahman, Amal Al Ghaferi: Hindawi J. Nanomater. 2017 (2017) 1. Research. DOI:10.1155/2017/6843403
[20] C.-X. Liu, J.-W. Choi: Nanomaterials. 2 (2012) 329. PMid:28348312; DOI:10.3390/nano2040329
[21] H.U. Bo-xing Zhang, Jun-Ichi Azuma: RSC Adv. J. 5 (2015) 2900. DOI:10.1039/c4ra14090 g
[22] H. Shim, M. Karina, R.Yudianti, L. Indrarti, J. Azuma, H. Uyama: Polym. Technol. Eng. 54 (2015) 305. DOI:10.1080/03602559.2014.977428
[23] R. Yudianti, A. Syampurwadi, H. Onggo, M. Karina, and H. Uyama: Polym. Adv. Technol. 27 (2016) 1102. DOI:10.1002/pat.3782
[24] R. Yudianti, H. Onggo, Sudirman, Y. Saito, T. Iwata, J. Azuma: Open Mater. Sci. J. 5 (2011) 242. DOI:10.2174/1874088X01105010242
[25] M.E. Hughes, E. Brandin, J.A. Golovchenko: Nanto Lett. 7 (2007) 1191. PMid:17419658; DOI:10.1021/nl062906u
[26] G. Wypych: "Photophysics," in Handbook of Material Weathering, 5th Editio., Science Direct, 2013, 744. DOI:10.1016/C2012-0-07343-7
[27] T.T. Nguyen, S.U. Nguyen, D.T. Phuong, D.C. Nguyen, and A.T. Mai: Adv. Nat. Sci. Nanosci. Nanotechnol. 2 (2011) 1. DOI:10.1088/2043-6262/2/3/035015
[28] M. Siegfried.: Compos. Struct., 452 – 453 (2013) 3593. DOI:10.1016/j.msea.2006.11.066
[29] Y. Zhang, J. Fang, J. Li, Y. Guo, Q. Wang: Polymers (Basel). 9 (2017). PMid:30966028; DOI:10.3390/polym9120728
[30] P. Pötschke, M.H. Arnaldo, H.J. Radusch: Polimery/Polymers 57 (2012) 204. DOI:10.14314/polimery.2012.204
[31] H. Abbasi, M. Antunes, J.I. Velasco: Polymers (Basel). 10 (2018) 1. PMid:30966383; DOI:10.3390/polym10040348
[32] I.V. Zaporotskova, N.P. Boroznina, Y.N. Parkhomenko, L.V. Kozhitov: Mod. Electron. Mater. 2 (2016) 95. DOI:10.1016/j.moem.2017.02.002
[33] G. Zhou, J-H. Byun, Y. Oh, B-M. Jung, H-J. Cha, D-G. Seong, M-K. Um, S. Hyun. T-W. Chou: ACS Appl. Mater. Interfaces. 9 (2017) 4788. DOI:10.1021/acsami.6b12448
[34] K. Tsirka, L. Tzounis, A. Avgeropoulos, M. Liebscher, V. Mechtcherine, A.S. Paipetis: Compos. Sci. Technol. 165 (2018) 240. DOI:10.1016/j.compscitech.2018.07.003
[35] L.I. Nasibulina, I.V. Anoshkin, A.G. Nasibulin, A. Cwirzen, V. Penttala, E.I. Kauppinen: J. Nanomater. 2012 (2012) 1. DOI:10.1155/2012/169262
[36] S. Ghoshal: Fibers. 5 (2017) 40. DOI:10.3390/fib5040040
[37] K.E. Wise, C. Park, E.J. Siochi, J.S. Harrison: Chem. Phys. Lett. 391 (2004) 207. DOI:10.1016/j.cplett.2004.04.096

(Received June 24, 2019; accepted October 4, 2019; online since February 6, 2020)

Correspondence address

Dr. Rike Yudianti
Research Centre for Physics
Indonesian Institute of Sciences
South Tangerang 15314
Indonesia
Tel.: +62(21) 7560570
Fax.: +62(21) 7560554
E-mail: rike001@lipi.go.id; rikeyudianti@gmail.com
Website: fisika.lipi.go.id

Bibliography
DOI 10.3139/146.111875
Int. J. Mater. Res. (formerly Z. Metallkd.)
111 (2020) 3; page 197 – 203

ISSN 1862-5282